Sequential Monte Carlo Implementation of the Track-Oriented Marginal Multi-Bernoulli/Poisson Filter

Thomas Kropfreiter*, Florian Meyer†, and Franz Hlawatsch*

*Institute of Telecommunications, TU Wien, 1040 Vienna, Austria ({tkropfre,fhlawats}@nt.tuwien.ac.at)
†Centre for Maritime Research and Experimentation, La Spezia 19126, Italy (florian.meyer@cmre.nato.int)

***Abstract*—The TOMB/P filter [Williams, 2011, 2015] is an attractive method for multiobject tracking. However, its original formulation is computationally feasible only for linear-Gaussian system models, and it suffers from the track coalescence effect. Here, we propose a sequential Monte Carlo (SMC) implementation of the TOMB/P filter, termed the TOMB/P-SMC filter, which avoids these drawbacks. We demonstrate the performance of the TOMB/P-SMC filter in a challenging scenario with a nonlinear range-bearing measurement model, low probability of detection, strong clutter, and intersecting objects. It is observed that track coalescence is significantly reduced, and that the TOMB/P-SMC filter is able to outperform SMC implementations of previously proposed filters such as the cardinalized PHD filter and the cardinality-balanced multi-Bernoulli filter.**

***Index Terms*—Multiobject tracking, multitarget tracking, data association, random finite set, FISST, TOMB/P filter.**

I. Introduction

A. State of the Art

For multiobject tracking, filters based on random finite sets (RFSs) and finite set statistics (FISST) are attractive solutions [1], [2]. Existing FISST-based methods include the probability hypothesis density (PHD) filter [1], [3], [4], the cardinalized PHD (CPHD) filter [1], [5], [6], and the cardinality-balanced multi-Bernoulli (CBMB) filter [1], [7]. A feasible sequential Monte Carlo (SMC) implementation of the (C)PHD filter [4], [6] involves a potentially unreliable clustering step. The CBMB filter does not require a clustering step but uses an approximation that is inaccurate in certain cases [7].

A recently proposed type of FISST-based filters avoids certain approximations used in the (C)PHD and CBMB filters by representing the posterior multiobject probability density function (pdf) as a specific mixture of multi-Bernoulli pdfs that is a conjugate-prior form of the posterior multiobject pdf [8]–[15]. However, this conjugate-prior representation involves a probability expansion with an excessive number of terms. In [8] and [13], a less complex filter—termed the track-oriented marginal multi-Bernoulli/Poisson (TOMB/P) filter—is obtained by assuming that the global association probabilities factorize into the marginal association probabilities, by computing the latter via belief propagation [16], and by modeling undetected objects by a Poisson process. A similar filter, which is however not based on FISST and belief propagation, is presented in [17]. An extension of the TOMB/P filter [9] summarizes Bernoulli components with a small existence probability as undetected objects, which makes it possible to keep the number of Bernoulli components fixed. In [15], a method that approximates the posterior multiobject pdf by a multi-Bernoulli pdf with a fixed number of Bernoulli components and aims at avoiding coalescence is proposed.

Another filter based on the conjugate-prior form is the generalized labeled multi-Bernoulli (GLMB) filter proposed in [10] and [11], which performs ordered (labeled) multiobject tracking. This filter uses a fixed number of expansion terms. Variants and extensions of the GLMB filter with reduced complexity are presented in [12] and [14].

B. Contribution and Paper Organization

The TOMB/P filter achieves excellent performance, automatically generates new potential objects (tracks), and scales well in the number of measurements and in the number of objects. However, it is computationally feasible only for linear-Gaussian systems. Here, we propose an SMC implementation of the TOMB/P filter, termed the TOMB/P-SMC filter, in which spatial distributions are represented by particles. This allows for arbitrary nonlinear, non-Gaussian systems and strongly reduces the track coalescence effect observed in the Gaussian mixture implementation of the TOMB/P filter [13]. We demonstrate the high accuracy of the TOMB/P-SMC filter in a challenging scenario with intersecting objects.

This paper is organized as follows. Some fundamentals of RFSs are reviewed next. The system model is described in Section II, and the TOMB/P filter is reviewed in Section III. The proposed TOMB/P-SMC filter is developed in Section IV. Simulation results are presented in Section V.

C. Some RFS Fundamentals

An RFS X is a random variable whose realizations X are finite sets $\{\mathbf{x}^{(1)}, \ldots, \mathbf{x}^{(n)}\}$ of vectors $\mathbf{x}^{(1)}, \ldots, \mathbf{x}^{(n)} \in \mathbb{R}^{n_x}$. Both the vectors $\mathbf{x}^{(i)}$ and their number $n = |X|$ (the cardinality of X) are chosen randomly. Thus, X consists of a random number n of random vectors $\mathbf{x}^{(1)}, \ldots, \mathbf{x}^{(\mathsf{n})}$. For $n = |X| = 0$, $X = \emptyset$. Adopting Mahler's FISST framework [1], an RFS X is described by its multiobject pdf $f_{\mathsf{X}}(X)$, briefly denoted

$f(X)$. For any realization $X = \{\mathbf{x}^{(1)}, \ldots, \mathbf{x}^{(n)}\}$ with a given cardinality $|X| = n$,

$$f(X) = n!\,\rho(n)\,f_n(\mathbf{x}^{(1)}, \ldots, \mathbf{x}^{(n)}). \quad (1)$$

Here, the *cardinality distribution* $\rho(n) \triangleq \Pr\{|\mathsf{X}| = n\}$, $n \in \mathbb{N}_0$ is the probability mass function (pmf) of the random cardinality $\mathsf{n} = |\mathsf{X}|$, and $f_n(\mathbf{x}^{(1)}, \ldots, \mathbf{x}^{(n)})$ is a pdf of the random vectors $\mathbf{x}^{(1)}, \ldots, \mathbf{x}^{(n)}$ (n fixed) that is invariant to a permutation of the arguments $\mathbf{x}^{(i)}$. In particular, $f(\emptyset) = \rho(0)$.

Next, we review three types of RFSs that are relevant to the TOMB/P filter. The cardinality of a *Poisson RFS* X is Poisson distributed with mean μ, i.e., $\rho(n) = e^{-\mu}\mu^n/n!$, $n \in \mathbb{N}_0$. Given $\mathsf{n} = n$, the elements $\mathbf{x}^{(1)}, \ldots, \mathbf{x}^{(n)}$ of X are independent and identically distributed (iid) according to a "spatial pdf" $f(\mathbf{x})$, i.e., $f_n(\mathbf{x}^{(1)}, \ldots, \mathbf{x}^{(n)}) = \prod_{i=1}^{n} f(\mathbf{x}^{(i)})$. Inserting into (1) then yields the multiobject pdf as

$$f(X) = e^{-\mu} \prod_{\mathbf{x} \in X} \mu f(\mathbf{x}).$$

The product $\mu f(\mathbf{x})$ is referred to as intensity function or PHD.

A *Bernoulli RFS* X with probability of existence r and spatial pdf $s(\mathbf{x})$ is empty with probability $1 - r$ and contains one element $\mathbf{x} \sim s(\mathbf{x})$ with probability r. Hence,

$$f(X) = \begin{cases} 1-r, & X = \emptyset, \\ r\,s(\mathbf{x}), & X = \{\mathbf{x}\}, \\ 0, & \text{otherwise.} \end{cases} \quad (2)$$

We note that $\sum_i \gamma_i f^{(i)}(X)$ with normalized γ_i (i.e., $\sum_i \gamma_i = 1$) and Bernoulli pdfs $f^{(i)}(X)$ is again a Bernoulli pdf.

A *multi-Bernoulli RFS* X is the union of independent Bernoulli RFSs $\mathsf{X}^{(i)}$, $i \in \{1, \ldots, I\}$ with existence probabilities $r^{(i)}$ and spatial pdfs $s^{(i)}(\mathbf{x})$, i.e., $\mathsf{X} = \bigcup_{i=1}^{I} \mathsf{X}^{(i)}$. The multiobject pdf $f(X)$ for $X = \{\mathbf{x}^{(1)}, \ldots, \mathbf{x}^{(n)}\}$ with $n \leq I$ is as follows [1], [13]. Consider a mapping α that maps n of the I Bernoulli components $\mathsf{X}^{(i)}$ to single-vector sets $\{\mathbf{x}^{(\alpha(i))}\}$ and the other $I - n$ Bernoulli components $\mathsf{X}^{(i)}$ to empty sets. More specificically, α maps an index $i \in \{1, \ldots, I\}$ to an index $\alpha(i) \in \{0, \ldots, n\}$, where $\alpha(i) = 0$ indicates that $\mathsf{X}^{(i)} = \emptyset$ and $\alpha(i) \in \{1, \ldots, n\}$ that $\mathsf{X}^{(i)} = \{\mathbf{x}^{(\alpha(i))}\}$. It is assumed that for i, j such that $\alpha(i), \alpha(j) \in \{1, \ldots, n\}$, $i \neq j$ implies $\alpha(i) \neq \alpha(j)$. Furthermore, let $\mathcal{P}_{I,n}$ denote the set of all such mappings α (there are $|\mathcal{P}_{I,n}| = I!/(I-n)!$ different mappings). Then,

$$f(X) = \sum_{\alpha \in \mathcal{P}_{I,n}} \prod_{i=1}^{I} f^{(i)}\big(X^{\alpha(i)}\big), \quad (3)$$

where $n = |X|$, $f^{(i)}(X)$ denotes the multiobject pdf of the ith Bernoulli component $\mathsf{X}^{(i)}$ (cf. (2)), and $X^{\alpha(i)}$ is $\emptyset$ for $\alpha(i) = 0$ and $\{\mathbf{x}^{(\alpha(i))}\}$ for $\alpha(i) \in \{1, \ldots, n\}$.

II. System Model

We use the standard system model for multiobject tracking with measurement origin uncertainty [1], [18]. At time $k \in \mathbb{N}_0$, there are N_k objects with states $\mathbf{x}_k^{(1)}, \ldots, \mathbf{x}_k^{(N_k)} \in \mathbb{R}^{n_x}$. Each state vector $\mathbf{x}_k^{(i)}$ consists of parameters such as position, velocity, etc. Furthermore, a sensor observes M_k measurements $\mathbf{z}_k^{(1)}, \ldots, \mathbf{z}_k^{(M_k)} \in \mathbb{R}^{n_z}$. Because the objects and measurements are both unordered, with N_k and M_k random and possibly time-varying, we model the object states and measurements as RFSs $\mathsf{X}_k \triangleq \{\mathbf{x}_k^{(1)}, \ldots, \mathbf{x}_k^{(\mathsf{N}_k)}\}$ and $\mathsf{Z}_k \triangleq \{\mathbf{z}_k^{(1)}, \ldots, \mathbf{z}_k^{(\mathsf{M}_k)}\}$.

A. State Evolution Model

An object with state $\mathbf{x}_{k-1}$ at time $k-1$ survives with probability $p_\mathrm{s}(\mathbf{x}_{k-1})$ and dies with probability $1 - p_\mathrm{s}(\mathbf{x}_{k-1})$. If it survives, its new state at time k is distributed according to $f(\mathbf{x}_k|\mathbf{x}_{k-1})$. Thus, each object that existed at time $k-1$ is modeled at time k as a Bernoulli RFS $\mathsf{S}_k(\mathbf{x}_{k-1})$ with existence probability $p_\mathrm{s}(\mathbf{x}_{k-1})$ and spatial pdf $f(\mathbf{x}_k|\mathbf{x}_{k-1})$ (cf. (2)). Assuming that the object states evolve independently, this results in the multi-Bernoulli RFS $\bigcup_{\mathbf{x}_{k-1} \in X_{k-1}} \mathsf{S}_k(\mathbf{x}_{k-1})$. In addition, new objects may be born. Following [13], we model the newborn objects as a Poisson RFS Γ_k with mean parameter μ_b, spatial pdf $b(\mathbf{x}_k)$, and corresponding intensity function $\lambda_\mathrm{b}(\mathbf{x}_k) = \mu_\mathrm{b} b(\mathbf{x}_k)$. The multiobject state RFS at time k, $\mathsf{X}_k = \{\mathbf{x}_k^{(1)}, \ldots, \mathbf{x}_k^{(\mathsf{N}_k)}\}$, then results as

$$\mathsf{X}_k = \left(\bigcup_{\mathbf{x}_{k-1} \in X_{k-1}} \mathsf{S}_k(\mathbf{x}_{k-1}) \right) \cup \Gamma_k.$$

This model defines the *RFS transition pdf* $f(X_k|X_{k-1})$.

B. Measurement Model

An existing object with state $\mathbf{x}_k$ is detected by the sensor with probability $p_\mathrm{d}(\mathbf{x}_k)$ and missed with probability $1 - p_\mathrm{d}(\mathbf{x}_k)$. If it is detected, it originates a measurement $\mathbf{z}_k^{(j)}$ according to the pdf $f(\mathbf{z}_k|\mathbf{x}_k)$ (likelihood function), and if it is not detected, it originates no measurement. Accordingly, the measurement originated by an object with state $\mathbf{x}_k$ is modeled as a Bernoulli RFS $\Theta_k(\mathbf{x}_k)$ with existence probability $p_\mathrm{d}(\mathbf{x}_k)$ and spatial pdf $f(\mathbf{z}_k|\mathbf{x}_k)$. We assume that each object-originated measurement is conditionally independent, given the respective object state, of all the other measurements and object states. Thus, the object-originated measurements form the multi-Bernoulli RFS $\bigcup_{\mathbf{x}_k \in X_k} \Theta_k(\mathbf{x}_k)$. In addition, measurements $\mathbf{z}_k^{(j)}$ may also be originated by clutter. Following [1], [13], we model the clutter-originated measurements as a Poisson RFS K_k with mean parameter μ_c, spatial pdf $f_\mathrm{c}(\mathbf{z}_k)$, and corresponding intensity function $\lambda_\mathrm{c}(\mathbf{z}_k) = \mu_\mathrm{c} f_\mathrm{c}(\mathbf{z}_k)$. Thus, the overall measurement RFS at time k, $\mathsf{Z}_k = \{\mathbf{z}_k^{(1)}, \ldots, \mathbf{z}_k^{(\mathsf{M}_k)}\}$, is obtained as

$$\mathsf{Z}_k = \left(\bigcup_{\mathbf{x}_k \in X_k} \Theta_k(\mathbf{x}_k) \right) \cup \mathsf{K}_k.$$

This model defines the *RFS likelihood function* $f(Z_k|X_k)$.

III. Review of the TOMB/P Filter

In a Bayesian RFS setting, multiobject state estimation relies on the marginal posterior pdf $f(X_k|Z_{1:k})$, where $Z_{1:k} \triangleq (Z_1, \ldots, Z_k)$. This pdf can be calculated recursively by means of a *prediction step*, which converts the previous

marginal posterior pdf $f(X_{k-1}|Z_{1:k-1})$ into a "predicted pdf" $f(X_k|Z_{1:k-1})$, and an *update step*, which converts $f(X_k|Z_{1:k-1})$ into $f(X_k|Z_{1:k})$. The prediction step involves the RFS transition pdf $f(X_k|X_{k-1})$, and the update step involves the RFS likelihood function $f(Z_k|X_k)$ and, thus, the current measurement Z_k. Different filters use different assumptions and approximations for computational feasibility. In this section, we review the TOMB/P filter introduced in [8], [13]. Derivations can be found in [13].

In the TOMB/P filter, conditioned on $\mathsf{Z}_{1:k}$, the multiobject state RFS X_k is modeled as the union of independent RFSs $\mathsf{X}_k^{\mathrm{u}}$ and $\mathsf{X}_k^{\mathrm{d}}$ describing the undetected and detected objects, respectively. Thus, the posterior multiobject pdf $f(X_k|Z_{1:k})$ is given by the FISST convolution [1]

$$f(X_k|Z_{1:k}) = \sum_{Y \subseteq X_k} f_{\mathrm{u}}(Y)\, f_{\mathrm{d}}(X_k \backslash Y), \tag{4}$$

where $f_{\mathrm{u}}(X_k)$ is the pdf of $\mathsf{X}_k^{\mathrm{u}}$ (note that $\mathsf{X}_k^{\mathrm{u}}$ is independent of $\mathsf{Z}_{1:k}$) and $f_{\mathrm{d}}(X_k)$ is the posterior pdf[1] of $\mathsf{X}_k^{\mathrm{d}}$. Here, $\mathsf{X}_k^{\mathrm{u}}$ is modeled by a Poisson RFS with mean parameter μ_{u}, spatial pdf $f_{\mathrm{u}}(\mathbf{x}_k)$, and intensity function $\lambda_{\mathrm{u}}(\mathbf{x}_k) = \mu_{\mathrm{u}} f_{\mathrm{u}}(\mathbf{x}_k)$. Furthermore, $\mathsf{X}_k^{\mathrm{d}}$ is modeled by a multi-Bernoulli RFS consisting of I_k Bernoulli components with existence probabilities $r_k^{(i)}$ and spatial pdfs $s^{(i)}(\mathbf{x}_k)$, $i \in \{1, \ldots, I_k\}$, where each Bernoulli component represents a *potential object* (PO).

A. Prediction Step

The prediction step of the TOMB/P filter preserves the convolution form (4), i.e., the predicted pdf $f(X_k|Z_{1:k-1})$ is again the convolution of a Poisson pdf $f^{\mathrm{u}}_{k|k-1}(X_k)$ and a multi-Bernoulli pdf $f^{\mathrm{d}}_{k|k-1}(X_k)$. These two pdfs can be predicted separately. Indeed, the intensity function $\lambda^{\mathrm{u}}_{k|k-1}(\mathbf{x}_k)$ characterizing $f^{\mathrm{u}}_{k|k-1}(X_k)$ is calculated from the intensity function $\lambda_{\mathrm{u}}(\mathbf{x}_{k-1})$ characterizing $f_{\mathrm{u}}(X_{k-1})$ as

$$\lambda^{\mathrm{u}}_{k|k-1}(\mathbf{x}_k) = \lambda_{\mathrm{b}}(\mathbf{x}_k) + \int f(\mathbf{x}_k|\mathbf{x}_{k-1}) p_{\mathrm{s}}(\mathbf{x}_{k-1}) \times \lambda_{\mathrm{u}}(\mathbf{x}_{k-1})\, \mathrm{d}\mathbf{x}_{k-1}. \tag{5}$$

Furthermore, the parameters $r^{(i)}_{k|k-1}$ and $s^{(i)}_{k|k-1}(\mathbf{x}_k)$ characterizing $f^{\mathrm{d}}_{k|k-1}(X_k)$ are calculated from the parameters $r^{(i)}_{k-1}$ and $s^{(i)}(\mathbf{x}_{k-1})$ characterizing $f_{\mathrm{d}}(X_{k-1})$ as

$$r^{(i)}_{k|k-1} = r^{(i)}_{k-1} \int p_{\mathrm{s}}(\mathbf{x}_{k-1})\, s^{(i)}(\mathbf{x}_{k-1})\, \mathrm{d}\mathbf{x}_{k-1}, \tag{6}$$

$$s^{(i)}_{k|k-1}(\mathbf{x}_k) = \frac{\int f(\mathbf{x}_k|\mathbf{x}_{k-1})\, p_{\mathrm{s}}(\mathbf{x}_{k-1})\, s^{(i)}(\mathbf{x}_{k-1})\, \mathrm{d}\mathbf{x}_{k-1}}{\int p_{\mathrm{s}}(\mathbf{x}_{k-1})\, s^{(i)}(\mathbf{x}_{k-1})\, \mathrm{d}\mathbf{x}_{k-1}}, \tag{7}$$

for $i \in \{1, \ldots, I_{k-1}\}$. Note that the number of Bernoulli components I_{k-1} is not changed by the prediction step.

[1]We note that $f_{\mathrm{d}}(X_k)$ is short for $f_{\mathrm{d}}(X_k|Z_{1:k})$. We will often omit the condition $Z_{1:k}$ also in other posterior pdfs and probabilities to simplify the notation.

B. Update Step: Exact Version

The update step for the undetected objects yields again a Poisson pdf $f_{\mathrm{u}}(X_k)$, whose intensity function $\lambda_{\mathrm{u}}(\mathbf{x}_k)$ is calculated from $\lambda^{\mathrm{u}}_{k|k-1}(\mathbf{x}_k)$ as

$$\lambda_{\mathrm{u}}(\mathbf{x}_k) = (1 - p_{\mathrm{d}}(\mathbf{x}_k))\, \lambda^{\mathrm{u}}_{k|k-1}(\mathbf{x}_k). \tag{8}$$

However, the update step for the detected objects yields a *weighted mixture* of multi-Bernoulli pdfs. (An approximation resulting again in a multi-Bernoulli pdf will be reviewed in Section III-C.) The maximally possible number of Bernoulli components (i.e., POs) per mixture component is

$$I_k = I_{k-1} + M_k,$$

consisting of one "legacy" PO $i \in \{1, \ldots, I_{k-1}\}$ for each predicted PO and one new PO $i \in \{I_{k-1}+1, \ldots, I_{k-1}+M_k\}$ for each of the M_k measurements $\mathbf{z}_k^{(j)}$, $j \in \{1, \ldots, M_k\}$.

An expression of $f_{\mathrm{d}}(X_k)$ can be obtained by first introducing the PO-measurement association vector $\mathbf{a} = [a_1 \cdots a_{I_k}]^{\mathrm{T}}$. Here, $a_i = 0$ indicates that PO i is not associated with any measurement. Furthermore, for $i \in \{1, \ldots, I_{k-1}\}$, $a_i = j \in \{1, \ldots, M_k\}$ indicates that *legacy* PO i is associated with measurement j. Finally, for $i = I_{k-1} + j$ with $j \in \{1, \ldots, M_k\}$, $a_i = a_{I_{k-1}+j} = j$ indicates that *new* PO j is associated with measurement j (note that a new PO can only be associated with the measurement from which it was created). We have $\mathbf{a} \in \mathcal{A}_k$, where the association alphabet $\mathcal{A}_k$ contains all admissible PO-measurement association events at time k. Here, admissible means that each measurement is associated with exactly one (legacy or new) PO. One now obtains

$$f_{\mathrm{d}}(X_k) = \sum_{\mathbf{a} \in \mathcal{A}_k} p_k(\mathbf{a})\, f^{\mathrm{MB}}_{\mathbf{a}}(X_k), \tag{9}$$

where $p_k(\mathbf{a})$ is the probability of association event $\mathbf{a}$ and $f^{\mathrm{MB}}_{\mathbf{a}}(X_k)$ is a multi-Bernoulli pdf. Thus, $f_{\mathrm{d}}(X_k)$ is a mixture of multi-Bernoulli pdfs $f^{\mathrm{MB}}_{\mathbf{a}}(X_k)$, $\mathbf{a} \in \mathcal{A}_k$ with weights $p_k(\mathbf{a})$. The association probabilities factorize as

$$p_k(\mathbf{a}) \propto \prod_{i=1}^{I_k} \beta_k^{(i,a_i)}, \quad \mathbf{a} \in \mathcal{A}_k. \tag{10}$$

Finally, using (3) in (9) yields

$$f_{\mathrm{d}}(X_k) = \sum_{\mathbf{a} \in \mathcal{A}_k} p_k(\mathbf{a}) \sum_{\alpha \in \mathcal{P}_{I_k, n_k}} \prod_{i=1}^{I_k} f^{(i,a_i)}\big(X_k^{\alpha(i)}\big), \tag{11}$$

where $n_k = |X_k|$ and $f^{(i,a_i)}(X)$ is the pdf of the Bernoulli component corresponding to PO i and association variable a_i.

The update step now amounts to calculating the "association weights" $\beta_k^{(i,a_i)}$ in (10) as well as the existence probabilities $r_k^{(i,a_i)}$ and spatial distributions $s^{(i,a_i)}(\mathbf{x}_k)$ characterizing the Bernoulli components $f^{(i,a_i)}(X_k)$ in (11). For the legacy POs $i \in \{1, \ldots, I_{k-1}\}$, the association weights are given by

$$\beta_k^{(i,0)} = 1 - r^{(i)}_{k|k-1} + r^{(i)}_{k|k-1} \int (1 - p_{\mathrm{d}}(\mathbf{x}_k))\, s^{(i)}_{k|k-1}(\mathbf{x}_k)\, \mathrm{d}\mathbf{x}_k \tag{12}$$

and

$$\beta_k^{(i,a_i)} = r_{k|k-1}^{(i)} \int f\big(\mathbf{z}_k^{(a_i)}\big|\mathbf{x}_k\big)\, p_{\mathrm{d}}(\mathbf{x}_k)\, s_{k|k-1}^{(i)}(\mathbf{x}_k)\,\mathrm{d}\mathbf{x}_k \quad (13)$$

for $a_i \in \{1,\ldots,M_k\}$; the existence probabilities are given by

$$r_k^{(i,0)} = \frac{r_{k|k-1}^{(i)} \int (1-p_{\mathrm{d}}(\mathbf{x}_k))\, s_{k|k-1}^{(i)}(\mathbf{x}_k)\,\mathrm{d}\mathbf{x}_k}{1 - r_{k|k-1}^{(i)} + r_{k|k-1}^{(i)} \int (1-p_{\mathrm{d}}(\mathbf{x}_k))\, s_{k|k-1}^{(i)}(\mathbf{x}_k)\,\mathrm{d}\mathbf{x}_k} \quad (14)$$

and $r_k^{(i,a_i)} = 1$ for $a_i \in \{1,\ldots,M_k\}$; and the spatial distributions are given by

$$s^{(i,0)}(\mathbf{x}_k) = \frac{(1-p_{\mathrm{d}}(\mathbf{x}_k))\, s_{k|k-1}^{(i)}(\mathbf{x}_k)}{\int (1-p_{\mathrm{d}}(\mathbf{x}'_k))\, s_{k|k-1}^{(i)}(\mathbf{x}'_k)\,\mathrm{d}\mathbf{x}'_k} \quad (15)$$

and

$$s^{(i,a_i)}(\mathbf{x}_k) = \frac{f\big(\mathbf{z}_k^{(a_i)}\big|\mathbf{x}_k\big)\, p_{\mathrm{d}}(\mathbf{x}_k)\, s_{k|k-1}^{(i)}(\mathbf{x}_k)}{\int f\big(\mathbf{z}_k^{(a_i)}\big|\mathbf{x}'_k\big)\, p_{\mathrm{d}}(\mathbf{x}'_k)\, s_{k|k-1}^{(i)}(\mathbf{x}'_k)\,\mathrm{d}\mathbf{x}'_k} \quad (16)$$

for $a_i \in \{1,\ldots,M_k\}$. For the new POs $i = I_{k-1}+j$, $j \in \{1,\ldots,M_k\}$, we recall that $a_i \in \{0, j\}$. Here, the association weights are given by $\beta_k^{(i,0)} = 1$ and

$$\beta_k^{(i,j)} = \lambda_{\mathrm{c}}\big(\mathbf{z}_k^{(j)}\big) + \int f\big(\mathbf{z}_k^{(j)}\big|\mathbf{x}_k\big)\, p_{\mathrm{d}}(\mathbf{x}_k)\, \lambda_{k|k-1}^{\mathrm{u}}(\mathbf{x}_k)\,\mathrm{d}\mathbf{x}_k\,; \quad (17)$$

the existence probabilities are given by $r_k^{(i,0)} = 0$ and

$$r_k^{(i,j)} = \frac{\int f\big(\mathbf{z}_k^{(j)}\big|\mathbf{x}_k\big)\, p_{\mathrm{d}}(\mathbf{x}_k)\, \lambda_{k|k-1}^{\mathrm{u}}(\mathbf{x}_k)\,\mathrm{d}\mathbf{x}_k}{\lambda_{\mathrm{c}}\big(\mathbf{z}_k^{(j)}\big) + \int f\big(\mathbf{z}_k^{(j)}\big|\mathbf{x}_k\big)\, p_{\mathrm{d}}(\mathbf{x}_k)\, \lambda_{k|k-1}^{\mathrm{u}}(\mathbf{x}_k)\,\mathrm{d}\mathbf{x}_k}\,; \quad (18)$$

and the spatial distributions are given by (note that $s^{(i,0)}(\mathbf{x}_k)$ does not exist since for $a_i = 0$ no new PO has been generated)

$$s^{(i,j)}(\mathbf{x}_k) = \frac{f\big(\mathbf{z}_k^{(j)}\big|\mathbf{x}_k\big)\, p_{\mathrm{d}}(\mathbf{x}_k)\, \lambda_{k|k-1}^{\mathrm{u}}(\mathbf{x}_k)}{\int f\big(\mathbf{z}_k^{(j)}\big|\mathbf{x}'_k\big)\, p_{\mathrm{d}}(\mathbf{x}'_k)\, \lambda_{k|k-1}^{\mathrm{u}}(\mathbf{x}'_k)\,\mathrm{d}\mathbf{x}'_k}\,. \quad (19)$$

C. Update Step: Approximation

The TOMB/P filter employs certain approximations to preserve the multi-Bernoulli form in the update step $f_{k|k-1}^{\mathrm{d}}(X_k) \to f_{\mathrm{d}}(X_k)$ [13]. First, an extended association alphabet $\tilde{\mathcal{A}}_k$ is used that includes also inadmissible PO-measurement associations $\mathbf{a}$ (i.e., a measurement may be associated with no PO or with more than one PO). The pmf of $\mathbf{a}$ on $\tilde{\mathcal{A}}_k$ is defined as

$$\tilde{p}_k(\mathbf{a}) \triangleq \begin{cases} p_k(\mathbf{a}) \propto \prod_{i=1}^{I_k} \beta_k^{(i,a_i)}, & \mathbf{a} \in \mathcal{A}_k \\ 0, & \mathbf{a} \in \tilde{\mathcal{A}}_k \backslash \mathcal{A}_k\,, \end{cases} \quad (20)$$

where (10) was used. Even though $\tilde{p}_k(\mathbf{a})$ no longer factorizes as did $p_k(\mathbf{a})$, it is approximated by the product of the marginal association probabilities corresponding to $\tilde{p}_k(\mathbf{a})$. That is,

$$\tilde{p}_k(\mathbf{a}) \approx \prod_{i=1}^{I_k} p_k^{(i)}(a_i), \quad \mathbf{a} \in \tilde{\mathcal{A}}_k\,, \quad (21)$$

with

$$p_k^{(i)}(a_i) \triangleq \sum_{\sim a_i} \tilde{p}_k(\mathbf{a}) = \sum_{\sim a_i} p_k(\mathbf{a}), \quad (22)$$

where the summation is over all $a_{i'}$ with $i' \in \{1,\ldots,I_k\}\backslash\{i\}$. The complexity of this summation is exponential in I_k; however, accurate approximations of the $p_k^{(i)}(a_i)$ can be calculated efficiently by using a belief propagation algorithm [16]. The input to this algorithm are the $\beta_k^{(i,a_i)}$ (cf. (20)), which are calculated as discussed in Section III-B. Substituting $\tilde{\mathcal{A}}_k$ for $\mathcal{A}_k$ and $\tilde{p}_k(\mathbf{a})$ for $p_k(\mathbf{a})$ in (11) and using (21) yields

$$\begin{aligned} \tilde{f}_{\mathrm{d}}(X_k) &\triangleq \sum_{\mathbf{a}\in\tilde{\mathcal{A}}_k} \tilde{p}_k(\mathbf{a}) \sum_{\alpha\in\mathcal{P}_{I_k,n_k}} \prod_{i=1}^{I_k} f^{(i,a_i)}\big(X_k^{\alpha(i)}\big) \\ &\approx \sum_{\alpha\in\mathcal{P}_{I_k,n_k}} \prod_{i=1}^{I_k} \sum_{a_i} p_k^{(i)}(a_i)\, f^{(i,a_i)}\big(X_k^{\alpha(i)}\big)\,. \end{aligned}$$

Here, the identity $\sum_{\mathbf{a}\in\tilde{\mathcal{A}}_k} \prod_{i=1}^{I_k} p_k^{(i)}(a_i) = \prod_{i=1}^{I_k} \sum_{a_i} p_k^{(i)}(a_i)$ was used. Because $f^{(i)}(X_k) \triangleq \sum_{a_i} p_k^{(i)}(a_i) f^{(i,a_i)}\big(X_k^{\alpha(i)}\big)$ is again a Bernoulli pdf, $\tilde{f}_{\mathrm{d}}(X_k)$ is a multi-Bernoulli pdf (cf. (3)), consisting of the $I_k = I_{k-1} + M_k$ Bernoulli components $f^{(i)}(X_k)$, $i \in \{1,\ldots,I_k\}$.

The multi-Bernoulli pdf $\tilde{f}_{\mathrm{d}}(X_k)$ is characterized by the parameters $r_k^{(i)}$ and $s^{(i)}(\mathbf{x}_k)$ characterizing the Bernoulli components $f^{(i)}(X_k)$, $i \in \{1,\ldots,I_k\}$. Therefore, the update step for the POs now amounts to calculating these parameters from $\lambda_{k|k-1}^{\mathrm{u}}(\mathbf{x}_k)$ and from $r_{k|k-1}^{(i)}$ and $s_{k|k-1}^{(i)}(\mathbf{x}_k)$, $i \in \{1,\ldots, I_{k-1}\}$. For the legacy POs $i \in \{1,\ldots,I_{k-1}\}$, one obtains

$$r_k^{(i)} = \sum_{a_i=0}^{M_k} p_k^{(i)}(a_i)\, r_k^{(i,a_i)}, \quad (23)$$

$$s^{(i)}(\mathbf{x}_k) = \frac{1}{r_k^{(i)}} \sum_{a_i=0}^{M_k} p_k^{(i)}(a_i)\, r_k^{(i,a_i)} s^{(i,a_i)}(\mathbf{x}_k), \quad (24)$$

and for the new POs $i = I_{k-1} + j$ with $j \in \{1,\ldots,M_k\}$,

$$r_k^{(i)} = p_k^{(i)}(j)\, r_k^{(i,j)}, \quad (25)$$

$$s^{(i)}(\mathbf{x}_k) = s^{(i,j)}(\mathbf{x}_k). \quad (26)$$

We recall that expressions of $r_k^{(i,a_i)}$ and $s^{(i,a_i)}(\mathbf{x}_k)$ (involving $\lambda_{k|k-1}^{\mathrm{u}}(\mathbf{x}_k)$, $r_{k|k-1}^{(i)}$, and $s_{k|k-1}^{(i)}(\mathbf{x}_k)$) were provided in Section III-B. Since $I_k = I_{k-1} + M_k$, the number of Bernoulli components (POs) would increase in the kth update step by M_k. In practice, typically, a pruning is employed whereby only the Bernoulli components with $r_k^{(i)}$ larger than a threshold $P_{\mathrm{th}}^{\mathrm{p}}$ are used in the next prediction step. That is, I_k is redefined to be the number of these dominant Bernoulli components.

D. Detection and Estimation

PO i is considered to exist at time k if $r_k^{(i)}$ is larger than a threshold $P_{\mathrm{th}}^{\mathrm{d}}$. For each PO i that is considered to exist, an

estimate of the object state $\mathbf{x}_k^{(i)}$ is calculated as

$$\hat{\mathbf{x}}_k^{(i)} \triangleq \int \mathbf{x}_k \, s^{(i)}(\mathbf{x}_k) \, \mathrm{d}\mathbf{x}_k. \tag{27}$$

IV. Sequential Monte Carlo Implementation

We now develop the proposed TOMB/P-SMC filter. The original TOMB/P filter [13] obtains computationally feasible implementations of the prediction and update steps in Section III by modeling the spatial pdfs of the POs as Gaussians and the intensity function of the undetected objects as a mixture of Gaussians, and by assuming linear-Gaussian state evolution and measurement models. The proposed TOMB/P-SMC filter overcomes these restrictions by using particle representations of spatial pdfs and intensity functions and by performing Monte Carlo integration. It is thus suited to nonlinear, non-Gaussian state evolution and measurement models. Our development uses basic SMC principles presented in [19]–[21].

A. Prediction Step

1) Undetected Objects: The previous intensity function $\lambda_{\mathrm{u}}(\mathbf{x}_{k-1})$ involved in the prediction relation (5) is represented by L_{u} weighted particles $\big\{\big(\mathbf{x}_{\mathrm{u},k-1}^{(l)}, w_{\mathrm{u},k-1}^{(l)}\big)\big\}_{l=1}^{L_{\mathrm{u}}}$, which were calculated at time $k-1$. Contrary to standard particle filtering, $\sum_{l=1}^{L_{\mathrm{u}}} w_{\mathrm{u},k-1}^{(l)}$ is not 1 in general but approximates the expected number of undetected objects, $\int \lambda_{\mathrm{u}}(\mathbf{x}_{k-1}) \, \mathrm{d}\mathbf{x}_{k-1} = \mu_{\mathrm{u}}$. The particle representation $\big\{\big(\mathbf{x}_{\mathrm{u},k-1}^{(l)}, w_{\mathrm{u},k-1}^{(l)}\big)\big\}_{l=1}^{L_{\mathrm{u}}}$ of $\lambda_{\mathrm{u}}(\mathbf{x}_{k-1})$ is now converted into a particle representation $\big\{\big(\mathbf{x}_{\mathrm{u},k|k-1}^{(l)}, w_{\mathrm{u},k|k-1}^{(l)}\big)\big\}_{l=1}^{L'_{\mathrm{u}}}$ of the predicted intensity function $\lambda_{k|k-1}^{\mathrm{u}}(\mathbf{x}_k)$, where $L'_{\mathrm{u}} > L_{\mathrm{u}}$. This prediction step comprises the prediction of existing particles and the generation of new particles representing new undetected objects.

Regarding the undetected objects that existed at time $k-1$ and survived to time k, for each particle $\mathbf{x}_{\mathrm{u},k-1}^{(l)}$, one particle $\mathbf{x}_{\mathrm{u},k|k-1}^{(l)}$ is drawn from $f\big(\mathbf{x}_k \big| \mathbf{x}_{\mathrm{u},k-1}^{(l)}\big)$, and a corresponding weight $w_{\mathrm{u},k|k-1}^{(l)}$ is calculated as (cf. the last term in (5))

$$w_{\mathrm{u},k|k-1}^{(l)} = f\big(\mathbf{x}_{\mathrm{u},k|k-1}^{(l)} \big| \mathbf{x}_{\mathrm{u},k-1}^{(l)}\big) \, p_{\mathrm{s}}\big(\mathbf{x}_{\mathrm{u},k-1}^{(l)}\big) \, w_{\mathrm{u},k-1}^{(l)},$$

for $l \in \{1, \ldots, L_{\mathrm{u}}\}$. In addition (cf. the first term on the right-hand side of (5)), J particles $\mathbf{x}_{\mathrm{u},k|k-1}^{(l)}$, $l \in \{L_{\mathrm{u}}+1, \ldots, L_{\mathrm{u}}+J\}$ for new undetected objects that did not exist at time $k-1$ are drawn from $b(\mathbf{x}_k)$, and corresponding weights are obtained as $w_{\mathrm{u},k|k-1}^{(l)} = \mu_{\mathrm{b}}/J$. The weighted particles $\big\{\big(\mathbf{x}_{\mathrm{u},k|k-1}^{(l)}, w_{\mathrm{u},k|k-1}^{(l)}\big)\big\}_{l=1}^{L'_{\mathrm{u}}}$, with $L'_u = L_u + J$, now represent $\lambda_{k|k-1}^{\mathrm{u}}(\mathbf{x}_k)$ in (5). If it is difficult to sample from $f\big(\mathbf{x}_k \big| \mathbf{x}_{\mathrm{u},k-1}^{(l)}\big)$ or $b(\mathbf{x}_k)$, then importance sampling can be used [21]. Here, the proposal pdf should not involve any measurements, since undetected objects are not measured—note that the TOMB/P filter already treats each measurement as a new PO by creating a new Bernoulli component as discussed in Section III-B.

2) POs: Next, we consider the prediction relations (6) and (7) for PO i. The previous spatial pdf $s^{(i)}(\mathbf{x}_{k-1})$ involved in these relations is represented by L weighted particles $\big\{\big(\mathbf{x}_{k-1}^{(i,l)}, w_{k-1}^{(i,l)}\big)\big\}_{l=1}^{L}$, which were calculated at time $k-1$. For each PO i, the previous existence probability $r_{k-1}^{(i)}$ and the particle representation $\big\{\big(\mathbf{x}_{k-1}^{(i,l)}, w_{k-1}^{(i,l)}\big)\big\}_{l=1}^{L}$ of $s^{(i)}(\mathbf{x}_{k-1})$ are now converted into a predicted existence probability $r_{k|k-1}^{(i)}$ and a particle representation $\big\{\big(\mathbf{x}_{k|k-1}^{(i,l)}, w_{k|k-1}^{(i,l)}\big)\big\}_{l=1}^{L}$ of the predicted spatial pdf $s_{k|k-1}^{(i)}(\mathbf{x}_k)$. We obtain $r_{k|k-1}^{(i)}$ by evaluating (6) via Monte Carlo integration, i.e.,

$$r_{k|k-1}^{(i)} = r_{k-1}^{(i)} \sum_{l=1}^{L} p_{\mathrm{s}}\big(\mathbf{x}_{k-1}^{(i,l)}\big) \, w_{k-1}^{(i,l)}. \tag{28}$$

(We still use the notation $r_{k|k-1}^{(i)}$ although (28) provides only an approximation, and similarly for all other Monte Carlo approximations.) Furthermore, for each particle $\mathbf{x}_{k-1}^{(i,l)}$, one particle $\mathbf{x}_{k|k-1}^{(i,l)}$ is drawn from $f\big(\mathbf{x}_k \big| \mathbf{x}_{k-1}^{(i,l)}\big)$, and corresponding weights $w_{k|k-1}^{(i,l)}$ are obtained by calculating (cf. (7))

$$\tilde{w}_{k|k-1}^{(i,l)} = p_{\mathrm{s}}\big(\mathbf{x}_{k-1}^{(i,l)}\big) \, w_{k-1}^{(i,l)}$$

and normalizing, i.e., $w_{k|k-1}^{(i,l)} = \tilde{w}_{k|k-1}^{(i,l)} / \sum_{l'=1}^{L} \tilde{w}_{k|k-1}^{(i,l')}$. The weighted particles $\big\{\big(\mathbf{x}_{k|k-1}^{(i,l)}, w_{k|k-1}^{(i,l)}\big)\big\}_{l=1}^{L}$ now represent $s_{k|k-1}^{(i)}(\mathbf{x}_k)$ in (7). Thus, the Bernoulli component corresponding to a predicted PO i is represented by $r_{k|k-1}^{(i)}$ in (28) and by $\big\{\big(\mathbf{x}_{k|k-1}^{(i,l)}, w_{k|k-1}^{(i,l)}\big)\big\}_{l=1}^{L}$. We note that a different choice of the proposal pdf [21] may lead to a reduction of the number of particles that are needed for accurate representations.

B. Update Step

1) Undetected Objects: The update step for the undetected objects converts the particle representation $\big\{\big(\mathbf{x}_{\mathrm{u},k|k-1}^{(l)}, w_{\mathrm{u},k|k-1}^{(l)}\big)\big\}_{l=1}^{L'_{\mathrm{u}}}$ of the predicted intensity function $\lambda_{k|k-1}^{\mathrm{u}}(\mathbf{x}_k)$ (see Section IV-A1) into a particle representation $\big\{\big(\mathbf{x}_{\mathrm{u},k}^{(l)}, w_{\mathrm{u},k}^{(l)}\big)\big\}_{l=1}^{L_{\mathrm{u}}}$ of $\lambda_{\mathrm{u}}(\mathbf{x}_k)$ in (8). This update step basically equals that in an SMC implementation of the PHD filter [4] without measurements, i.e., we first set

$$\begin{aligned} \bar{\mathbf{x}}_{\mathrm{u},k}^{(l)} &= \mathbf{x}_{\mathrm{u},k|k-1}^{(l)}, \\ \bar{w}_{\mathrm{u},k}^{(l)} &= \big(1 - p_{\mathrm{d}}\big(\mathbf{x}_{\mathrm{u},k}^{(l)}\big)\big) \, w_{\mathrm{u},k|k-1}^{(l)}, \end{aligned} \tag{29}$$

for $l \in \{1, \ldots, L'_{\mathrm{u}}\}$. Note that (29) corresponds to the update relation (8). Since the number of particles was increased in the prediction step from L_{u} to L'_{u}, we next apply resampling [19]–[21] to reduce the number of particles back to L_{u} and obtain the final particle representation $\big\{\big(\mathbf{x}_{\mathrm{u},k}^{(l)}, w_{\mathrm{u},k}^{(l)}\big)\big\}_{l=1}^{L_{\mathrm{u}}}$ of $\lambda_{\mathrm{u}}(\mathbf{x}_k)$. The resampling also counteracts particle degeneracy effects. Because $\hat{n}_k^{\mathrm{u}} \triangleq \sum_{l=1}^{L'_{\mathrm{u}}} \bar{w}_{\mathrm{u},k}^{(l)} \neq 1$ in general, the weights are divided by $\hat{n}_k^{\mathrm{u}}$ before resampling and multiplied by $\hat{n}_k^{\mathrm{u}}$ afterwards. As a consequence, the weights are obtained as $w_{\mathrm{u},k}^{(l)} = \hat{n}_k^{\mathrm{u}} / L_{\mathrm{u}}$. Details can be found in [4].

2) Legacy POs: The update step for the legacy POs $i \in \{1, \ldots, I_{k-1}\}$ converts the predicted existence probability $r_{k|k-1}^{(i)}$ and the particle representation $\big\{\big(\mathbf{x}_{k|k-1}^{(i,l)}, w_{k|k-1}^{(i,l)}\big)\big\}_{l=1}^{L}$

of the predicted spatial pdf $s_{k|k-1}^{(i)}(\mathbf{x}_k)$ (see Section IV-A2) into $r_k^{(i)}$ and a particle representation $\{(\mathbf{x}_k^{(i,l)}, w_k^{(i,l)})\}_{l=1}^{L}$ of $s^{(i)}(\mathbf{x}_k)$. To this end, we first calculate association weights $\beta_k^{(i,a_i)}$, existence probabilities $r_k^{(i,a_i)}$, and particle representations of the $s^{(i,a_i)}(\mathbf{x}_k)$ (see Section III-B).

For the case where an existing PO i is associated with some measurement $\mathbf{z}_k^{(a_i)}$, with $a_i \in \{1,\dots,M_k\}$, evaluating (13) via Monte Carlo integration gives

$$\beta_k^{(i,a_i)} = r_{k|k-1}^{(i)} \sum_{l=1}^{L} f\big(\mathbf{z}_k^{(a_i)}\big|\mathbf{x}_{k|k-1}^{(i,l)}\big)\, p_{\mathrm{d}}\big(\mathbf{x}_{k|k-1}^{(i,l)}\big)\, w_{k|k-1}^{(i,l)}. \quad (30)$$

According to Section III-B, $r_k^{(i,a_i)} = 1$. Finally, a particle representation $\{(\mathbf{x}_k^{(i,l)}, w_k^{(i,a_i,l)})\}_{l=1}^{L}$ of $s^{(i,a_i)}(\mathbf{x}_k)$ in (16) is obtained by first setting $\mathbf{x}_k^{(i,l)} = \mathbf{x}_{k|k-1}^{(i,l)}$ (note that this does not depend on a_i). Then, nonnormalized weights are calculated via Monte Carlo implementation of (16), i.e.,

$$\tilde{w}_k^{(i,a_i,l)} = f\big(\mathbf{z}_k^{(a_i)}\big|\mathbf{x}_k^{(i,l)}\big)\, p_{\mathrm{d}}\big(\mathbf{x}_k^{(i,l)}\big)\, w_{k|k-1}^{(i,l)},$$

and the final weights $w_k^{(i,a_i,l)}$ are obtained by normalization.

For the case where an existing PO i is not associated with any measurement ($a_i = 0$), using Monte Carlo integration in (12) and in (14) yields, respectively,

$$\beta_k^{(i,0)} = 1 - r_{k|k-1}^{(i)} + r_{k|k-1}^{(i)} \sum_{l=1}^{L} \big(1 - p_{\mathrm{d}}\big(\mathbf{x}_{k|k-1}^{(i,l)}\big)\big)\, w_{k|k-1}^{(i,l)} \quad (31)$$

and

$$r_k^{(i,0)} = \frac{r_{k|k-1}^{(i)} \sum_{l=1}^{L} \big(1 - p_{\mathrm{d}}\big(\mathbf{x}_{k|k-1}^{(i,l)}\big)\big)\, w_{k|k-1}^{(i,l)}}{1 - r_{k|k-1}^{(i)} + r_{k|k-1}^{(i)} \sum_{l=1}^{L} \big(1 - p_{\mathrm{d}}\big(\mathbf{x}_{k|k-1}^{(i,l)}\big)\big)\, w_{k|k-1}^{(i,l)}}.$$

Furthermore, a particle representation $\{(\mathbf{x}_k^{(i,l)}, w_k^{(i,0,l)})\}_{l=1}^{L}$ of $s^{(i,0)}(\mathbf{x}_k)$ in (15) is obtained by setting $\mathbf{x}_k^{(i,l)} = \mathbf{x}_{k|k-1}^{(i,l)}$ and calculating the $w_k^{(i,0,l)}$ as normalized versions of (cf. (15))

$$\tilde{w}_k^{(i,0,l)} = \big(1 - p_{\mathrm{d}}\big(\mathbf{x}_k^{(i,l)}\big)\big)\, w_{k|k-1}^{(i,l)}.$$

We are now able to calculate the existence probability $r_k^{(i)}$ of legacy PO $i \in \{1,\dots,I_{k-1}\}$. Using (23) while recalling that $r_k^{(i,a_i)} = 1$ for $a_i \in \{1,\dots,M_k\}$ yields

$$r_k^{(i)} = p_k^{(i)}(0)\, r_k^{(i,0)} + \sum_{a_i=1}^{M_k} p_k^{(i)}(a_i).$$

Furthermore, a particle representation $\{(\mathbf{x}_k^{(i,l)}, w_k^{(i,l)})\}_{l=1}^{L}$ of $s^{(i)}(\mathbf{x}_k)$ is obtained by using the particles $\mathbf{x}_k^{(i,l)} = \mathbf{x}_{k|k-1}^{(i,l)}$ and calculating the weights $w_k^{(i,l)}$ via Monte Carlo implementation of (24), i.e., as normalized versions of

$$\tilde{w}_k^{(i,l)} = p_k^{(i)}(0)\, r_k^{(i,0)}\, w_k^{(i,0,l)} + \sum_{a_i=1}^{M_k} p_k^{(i)}(a_i)\, w_k^{(i,a_i,l)}.$$

Resampling can now be applied to counteract particle degeneracy. The $p_k^{(i)}(a_i)$ are obtained by first calculating the association weights $\beta_k^{(i,a_i)}$ according to (30), (31), and (32). Then, the product in (20) and the marginalization (22) are computed efficiently via a belief propagation algorithm [16].

3) New POs: The update step for new POs $i = I_{k-1} + j$, $j \in \{1,\dots,M_k\}$ converts the particle representation $\{(\mathbf{x}_{\mathrm{u},k|k-1}^{(l)}, w_{\mathrm{u},k|k-1}^{(l)})\}_{l=1}^{L'_{\mathrm{u}}}$ of $\lambda_{k|k-1}^{\mathrm{u}}(\mathbf{x}_k)$ (see Section IV-A1) into an existence probability $r_k^{(i)}$ and a particle representation $\{(\mathbf{x}_k^{(i,l)}, w_k^{(i,l)})\}_{l=1}^{L}$ of $s^{(i)}(\mathbf{x}_k)$. As in Section IV-B2, we first calculate association weights $\beta_k^{(i,j)}$, existence probabilities $r_k^{(i,j)}$, and particle representations of the $s^{(i,j)}(\mathbf{x}_k)$ (see Section III-B). Because the shape of $f\big(\mathbf{z}_k^{(j)}\big|\mathbf{x}_k\big)$ is typically similar to that of $s^{(i,j)}(\mathbf{x}_k)$, we directly draw L equally weighted particles $\{\mathbf{x}_k^{(i,l)}\}_{l=1}^{L}$ from[2] $f\big(\mathbf{z}_k^{(j)}\big|\mathbf{x}_k\big)$. Then, using Monte Carlo integration in (17) and (18) yields, respectively,

$$\beta_k^{(i,j)} = \lambda_{\mathrm{c}}\big(\mathbf{z}_k^{(j)}\big) + \frac{C_j}{L} \sum_{l=1}^{L} p_{\mathrm{d}}\big(\mathbf{x}_k^{(i,l)}\big)\, \tilde{\lambda}_{k|k-1}^{\mathrm{u}}\big(\mathbf{x}_k^{(i,l)}\big) \quad (32)$$

and

$$r_k^{(i,j)} = \frac{\frac{C_j}{L} \sum_{l=1}^{L} p_{\mathrm{d}}\big(\mathbf{x}_k^{(i,l)}\big)\, \tilde{\lambda}_{k|k-1}^{\mathrm{u}}\big(\mathbf{x}_k^{(i,l)}\big)}{\lambda_{\mathrm{c}}\big(\mathbf{z}_k^{(j)}\big) + \frac{C_j}{L} \sum_{l=1}^{L} p_{\mathrm{d}}\big(\mathbf{x}_k^{(i,l)}\big)\, \tilde{\lambda}_{k|k-1}^{\mathrm{u}}\big(\mathbf{x}_k^{(i,l)}\big)}. \quad (33)$$

Here, $C_j \triangleq \int f\big(\mathbf{z}_k^{(j)}\big|\mathbf{x}_k\big)\, \mathrm{d}\mathbf{x}_k$ accounts for the fact that $\int f\big(\mathbf{z}_k^{(j)}\big|\mathbf{x}_k\big)\, \mathrm{d}\mathbf{x}_k \neq 1$ in general. (If C_j cannot be evaluated in closed form, it is computed by means of Monte Carlo integration [21].) Furthermore, $\tilde{\lambda}_{k|k-1}^{\mathrm{u}}(\mathbf{x}_k)$ is a kernel density approximation of $\lambda_{k|k-1}^{\mathrm{u}}(\mathbf{x}_k)$, which is calculated from the particle representation $\{(\mathbf{x}_{\mathrm{u},k|k-1}^{(l)}, w_{\mathrm{u},k|k-1}^{(l)})\}_{l=1}^{L'_{\mathrm{u}}}$ of $\lambda_{k|k-1}^{\mathrm{u}}(\mathbf{x}_k)$ according to $\tilde{\lambda}_{k|k-1}^{\mathrm{u}}(\mathbf{x}_k) = \sum_{l=1}^{L'_{\mathrm{u}}} w_{\mathrm{u},k|k-1}^{(l)} K\big(\mathbf{x}_k - \mathbf{x}_{\mathrm{u},k|k-1}^{(l)}\big)$. A standard choice of the kernel function $K(\cdot)$ is a multivariate Gaussian function with appropriate variances [22]. A particle representation of $s^{(i,j)}(\mathbf{x}_k)$ in (19) is now given by $\{(\mathbf{x}_k^{(i,l)}, w_k^{(i,l)})\}_{l=1}^{L}$, where the weights $w_k^{(i,l)}$ are calculated as normalized versions of (cf. (19))

$$\tilde{w}_k^{(i,l)} = p_{\mathrm{d}}\big(\mathbf{x}_k^{(i,l)}\big)\, \tilde{\lambda}_{k|k-1}^{\mathrm{u}}\big(\mathbf{x}_k^{(i,l)}\big). \quad (34)$$

Here, no resampling is required since we drew new particles from $f(\mathbf{z}_k^{(j)}|\mathbf{x}_k)$.

From $r_k^{(i,j)}$ in (33), the existence probability $r_k^{(i)}$ of new PO $i = I_{k-1} + j$, $j \in \{1,\dots,M_k\}$ is now obtained according to (25), i.e., $r_k^{(i)} = p_k^{(i)}(j)\, r_k^{(i,j)}$. Furthermore, according to (26), a particle representation of $s^{(i)}(\mathbf{x}_k)$ is given by the particle representation of $s^{(i,j)}(\mathbf{x}_k)$, i.e., by $\{(\mathbf{x}_k^{(i,l)}, w_k^{(i,l)})\}_{l=1}^{L}$.

C. Initialization

The recursion described in Sections IV-A and IV-B is initialized at time $k = 0$ by an initial particle set $\{(\mathbf{x}_{\mathrm{u},0}^{(l)}, w_{\mathrm{u},0}^{(l)})\}_{l=1}^{L_{\mathrm{u}}}$

[2] In those cases where $f(\mathbf{z}_k|\mathbf{x}_k)$ does not depend on some of the elements of $\mathbf{x}_k$, one can draw particles for these elements from a suitably chosen proposal pdf. This results in a slightly different calculation of the constant C_j in (32), (33) and of the weights in (34).

representing $\lambda_{\mathrm{u}}(\mathbf{x}_0) = \mu_{\mathrm{u}} f_{\mathrm{u}}(\mathbf{x}_0)$. Here, the $\mathbf{x}_{\mathrm{u},0}^{(l)}$ are drawn from a suitably chosen (e.g., uniform) initial prior pdf $f_{\mathrm{u}}(\mathbf{x}_0)$, and $w_{\mathrm{u},0}^{(l)} = \mu_{\mathrm{u}}/L_{\mathrm{u}}$. Furthermore, $I_0 = 0$ since there are no legacy POs at time $k = 0$.

D. Detection and Estimation

As in Section III-D, PO i is considered to exist at time k if $r_k^{(i)}$ is larger than a threshold $P_{\mathrm{th}}^{\mathrm{d}}$. In that case, an estimate of $\mathbf{x}_k^{(i)}$ is obtained via Monte Carlo implementation of (27), i.e.,

$$\hat{\mathbf{x}}_k^{(i)} = \sum_{l=1}^{L} \mathbf{x}_k^{(i,l)} w_k^{(i,l)}.$$

V. Numerical Study

We demonstrate the performance of the proposed TOMB/P-SMC filter in a challenging tracking scenario and compare it with that of three reference methods.

A. Simulation Setting

We consider a two-dimensional (2D) scenario with a region of interest (ROI) of $[-100, 100] \times [-100, 100]$. Six objects appear in the ROI at times $k = 10, 20, \ldots, 60$ and disappear at times $k = 140, 150, \ldots, 190$. The object states consist of 2D position and velocity, i.e., $\mathbf{x}_k = \begin{bmatrix} x_{1,k} & x_{2,k} & \dot{x}_{1,k} & \dot{x}_{2,k} \end{bmatrix}^{\mathrm{T}}$. The objects move independently according to the constant velocity motion model, i.e., $\mathbf{x}_k = \mathbf{A}\mathbf{x}_{k-1} + \mathbf{W}\mathbf{u}_k$, where $\mathbf{A} \in \mathbb{R}^{4\times 4}$ and $\mathbf{W} \in \mathbb{R}^{4\times 2}$ are chosen as in [23] and $\mathbf{u}_k \sim \mathcal{N}(\mathbf{0}, \sigma_u^2 \mathbf{I}_2)$ with $\sigma_u^2 = 0.01$ is an iid sequence of 2D Gaussian random vectors. The objects move towards the ROI center, where they all intersect around time $k = 100$. This behavior was obtained by generating all the object trajectories in the ROI center at time $k = 100$ and propagating the objects forward and backward in time. This trajectory generation scheme emphasizes the track coalescence effect; it was previously used in [13]. At time $k = 100$, the objects are distributed as $\mathbf{x}_{100} \sim \mathcal{N}(\mathbf{0}, 10^{-6}\mathbf{I}_4)$, which is a challenging case as the object states around time $k = 100$ are almost indistinguishable regarding both position and velocity. We set $p_{\mathrm{s}}(\mathbf{x}_{k-1}) = 0.999$ for all $\mathbf{x}_{k-1}$ and $\mu_{\mathrm{b}} = 0.01$. The birth pdf $b(\mathbf{x}_k)$ is uniform on the ROI.

We use the nonlinear range-bearing measurement model

$$\mathbf{z}_k^{(j)} = \begin{pmatrix} \left\| [x_{1,k} \ x_{2,k}]^{\mathrm{T}} - \mathbf{p} \right\| \\ \tan^{-1}\left(\frac{x_{1,k}-p_1}{x_{2,k}-p_2}\right) \end{pmatrix} + \mathbf{v}_k^{(j)}, \tag{35}$$

where $[x_{1,k} \ x_{2,k}]^{\mathrm{T}}$ is the position of a detected object, $\mathbf{p} = [p_1 \ p_2]^{\mathrm{T}} = [0 \ -100]^{\mathrm{T}}$ is the sensor position, and $\mathbf{v}_k^{(j)} \sim \mathcal{N}(\mathbf{0}, \mathrm{diag}\{\sigma_r^2, \sigma_\theta^2\})$ with $\sigma_r = 1$ and $\sigma_\theta = 0.5^\circ$ is an iid sequence of 2D Gaussian random vectors. The sensor has a measurement range of 200. The clutter pdf $f_{\mathrm{c}}(\mathbf{z}_k)$ is linearly increasing on $[0, 200]$ and zero outside $[0, 200]$ with respect to the range component and uniform on $[0, 360)$ with respect to the angle component. In Cartesian coordinates, this corresponds to a uniform distribution on the sensor's measurement area. We use $\mu_{\mathrm{c}} \in \{1, 5\}$ and $p_{\mathrm{d}}(\mathbf{x}_k) \in \{0.95, 0.75\}$. We performed 1000 simulation runs, each with 200 time steps.

B. Simulation Results

We compare the proposed TOMB/P-SMC filter with SMC implementations of the PHD [4], CPHD [6], and CBMB [7] filters. In the TOMB/P-SMC filter, each PO is represented by $L = 1000$ particles. (We observed no performance improvement for a larger number of particles.) The intensity function for undetected objects, $\lambda_{\mathrm{u}}(\mathbf{x}_k) = \mu_{\mathrm{u}} f_{\mathrm{u}}(\mathbf{x}_k)$, is initialized at time $k = 0$ by setting $\mu_{\mathrm{u}} = 1$ and choosing $f_{\mathrm{u}}(\mathbf{x}_0)$ as a uniform pdf. Because $p_{\mathrm{d}}(\mathbf{x}_k)$ and $p_{\mathrm{s}}(\mathbf{x}_{k-1})$ are state-independent and $b(\mathbf{x}_k)$ is uniform, $f_{\mathrm{u}}(\mathbf{x}_k)$ remains uniform after the prediction and update steps. Therefore, $\lambda_{k|k-1}^{\mathrm{u}}(\mathbf{x}_k)$ is a k-dependent constant, which can be easily evaluated, and thus a particle representation and a kernel density approximation of $\lambda_{k|k-1}^{\mathrm{u}}(\mathbf{x}_k)$ are not needed.

The birth intensities or pdfs of the PHD, CPHD, and CBMB filters are established using the previous measurements $\mathbf{z}_{k-1}^{(j)}$. More precisely, they are chosen as a mixture of components $f_{\mathrm{b}}^{(j)}(\mathbf{x}_k) = \frac{1}{C_j} \int f(\mathbf{x}_k|\mathbf{x}_{k-1}) f\big(\mathbf{z}_{k-1}^{(j)} \big| [x_{1,k-1} \ x_{2,k-1}]^{\mathrm{T}}\big) \times f_{\mathrm{v}}\big(\dot{x}_{1,k-1}, \dot{x}_{2,k-1}\big) \mathrm{d}\mathbf{x}_{k-1}$, $j \in \{1, \ldots, M_k\}$, where $f\big(\mathbf{z}_{k-1}^{(j)} \big| [x_{1,k-1} \ x_{2,k-1}]^{\mathrm{T}}\big)$ is the likelihood function corresponding to (35), $C_j \triangleq \int f\big(\mathbf{z}_{k-1}^{(j)} \big| [x_{1,k-1} \ x_{2,k-1}]^{\mathrm{T}}\big) \mathrm{d}x_{1,k-1} \mathrm{d}x_{2,k-1}$, and $f_{\mathrm{v}}\big(\dot{x}_{1,k-1}, \dot{x}_{2,k-1}\big) = \mathcal{N}(\mathbf{0}, 5^2\mathbf{I}_2)$. The PHD and CPHD filters use 6000 particles to represent the intensity function (PHD), of which 3000 represent the newborn objects. The latter particles are drawn from a mixture of the $f_{\mathrm{b}}^{(j)}(\mathbf{x}_k)$, $j \in \{1, \ldots, M_k\}$. State estimation in the PHD and CPHD filters is performed by using kmeans++ clustering [24]. The CBMB filter establishes a new PO (Bernoulli component) for each $\mathbf{z}_{k-1}^{(j)}$, with its spatial pdf represented by 1000 particles drawn from $f_{\mathrm{b}}^{(j)}(\mathbf{x}_k)$ and its existence probability set to $r_k = \mu_{\mathrm{b}}/M_{k-1}$. The TOMB/P-SMC and CBMB filters employ PO pruning (see Section III-C) with threshold $P_{\mathrm{th}}^{\mathrm{p}} = 10^{-6}$. The PO detection threshold (see Section III-D) is $P_{\mathrm{th}}^{\mathrm{d}} = 0.8$.

The performance of the various methods is measured by the Euclidean distance based mean OSPA (MOSPA) error [25] with cutoff parameter 20. Figs. 1(a) and (b) show the MOSPA error versus time k for $p_{\mathrm{d}}(\mathbf{x}_k) = 0.95$, $\mu_{\mathrm{c}} = 1$ and $p_{\mathrm{d}}(\mathbf{x}_k) = 0.75$, $\mu_{\mathrm{c}} = 5$, respectively. The peaks at $k = 10$, 20, etc. and 140, 150, etc. are due to the inability of the filters to detect the birth or death of objects instantaneously. The TOMB/P-SMC filter is seen to outperform the other filters at almost all times. The errors are generally larger in Fig. 1(b) due to the lower $p_{\mathrm{d}}(\mathbf{x}_k)$ and higher μ_{c}. The PHD and CPHD filters exhibit a temporary increase in the error around $k = 100$, i.e., when the object trajectories intersect. The TOMB/P-SMC filter, by contrast, exhibits a temporary increase in the error only after $k = 100$, i.e., when the objects move apart again. This behavior, known as track coalescence, can be observed in filters that use the approximation (21), such as the joint probabilistic data association filter [18] and related methods (e.g., [26]). However, a comparison of our results in Fig. 1 with those reported in [13], which were obtained for a linear-Gaussian scenario and a Gaussian mixture implementation of the TOMB/P filter, shows that the track coalescence effect is strongly reduced

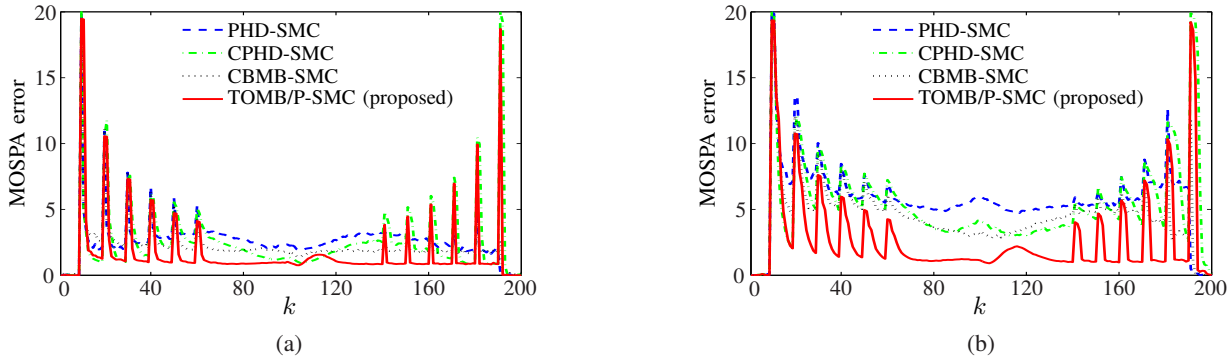

Fig. 1. MOSPA error versus time k: (a) for $p_{\mathrm{d}}(\mathbf{x}_k) = 0.95$ and $\mu_{\mathrm{c}} = 1$, (b) for $p_{\mathrm{d}}(\mathbf{x}_k) = 0.75$ and $\mu_{\mathrm{c}} = 5$.

by the proposed SMC implementation. This observation was confirmed by simulations (not shown) for the case where $\mathbf{z}_k^{(j)}$ equals the object position plus iid Gaussian noise.

VI. Conclusion

We proposed a sequential Monte Carlo (SMC) implementation of the TOMB/P filter, termed the TOMB/P-SMC filter, in which the spatial distributions of potential and undetected objects are represented by particles. In contrast to the original implementation of the TOMB/P filter [13], the TOMB/P-SMC filter is suited to general nonlinear, non-Gaussian state evolution and measurement models, and the effect of track coalescence observed in [13] is strongly reduced. We assessed the performance of the TOMB/P-SMC filter in a challenging scenario with a nonlinear measurement model and intersecting objects, and demonstrated that the TOMB/P-SMC filter can outperform three previously proposed filters. Possible directions for future research include extensions to multiple sensors and multiple detections per object.

Acknowledgments

This work was supported by the Austrian Science Fund (FWF) under grant P27370-N30 and by the National Sustainability Program of the European Commission under grant LO1401. F. Meyer is supported by the NATO Supreme Allied Command Transformation under project SAC000608.

References

[1] R. P. S. Mahler, *Statistical Multisource-Multitarget Information Fusion*. Boston, MA, USA: Artech House, 2007.

[2] ——, *Advances in Statistical Multisource-Multitarget Information Fusion*. Boston, MA, USA: Artech House, 2014.

[3] ——, "Multitarget Bayes filtering via first-order multitarget moments," *IEEE Trans. Aerosp. Electron. Syst.*, vol. 39, no. 4, pp. 1152–1178, Oct. 2003.

[4] B.-N. Vo, S. Singh, and A. Doucet, "Sequential Monte Carlo methods for multitarget filtering with random finite sets," *IEEE Trans. Aerosp. Electron. Syst.*, vol. 41, no. 4, pp. 1224–1245, Apr. 2005.

[5] R. P. S. Mahler, "PHD filters of higher order in target number," *IEEE Trans. Aerosp. Electron. Syst.*, no. 4, pp. 1523–1543, Oct. 2007.

[6] B.-T. Vo, B.-N. Vo, and A. Cantoni, "Analytic implementations of the cardinalized probability hypothesis density filter," *IEEE Trans. Signal Process.*, vol. 55, no. 7, pp. 3553–3567, Jul. 2007.

[7] ——, "The cardinality balanced multi-target multi-Bernoulli filter and its implementations," *IEEE Trans. Signal Process.*, vol. 57, no. 2, pp. 409–423, Feb. 2009.

[8] J. L. Williams, "Experiments with graphical model implementations of multiple target multiple Bernoulli filters," in *Proc. IEEE ISSNIP-11*, Adelaide, Australia, Dec. 2011, pp. 532–537.

[9] ——, "Hybrid Poisson and multi-Bernoulli filters," in *Proc. FUSION-12*, Singapore, Jul. 2012, pp. 1103–1110.

[10] B.-T. Vo and B.-N. Vo, "Labeled random finite sets and multi-object conjugate priors," *IEEE Trans. Signal Process.*, vol. 61, no. 13, pp. 3460–3475, Jul. 2013.

[11] B.-N. Vo, B.-T. Vo, and D. Phung, "Labeled random finite sets and the Bayes multi-target tracking filter," *IEEE Trans. Signal Process.*, vol. 62, no. 24, pp. 6554–6567, Dec. 2014.

[12] S. Reuter, B.-T. Vo, B.-N. Vo, and K. Dietmayer, "The labeled multi-Bernoulli filter," *IEEE Trans. Signal Process.*, vol. 62, no. 12, pp. 3246–3260, Jun. 2014.

[13] J. L. Williams, "Marginal multi-Bernoulli filters: RFS derivation of MHT, JIPDA, and association-based MeMBer," *IEEE Trans. Aerosp. Electron. Syst.*, vol. 51, no. 3, pp. 1664–1687, Jul. 2015.

[14] H. G. Hoang, B. T. Vo, and B.-N. Vo, "A fast implementation of the generalized labeled multi-Bernoulli filter with joint prediction and update," in *Proc. FUSION-15*, Washington, DC, USA, Jul. 2015, pp. 999–1006.

[15] J. L. Williams, "An efficient, variational approximation of the best fitting multi-Bernoulli filter," *IEEE Trans. Signal Process.*, vol. 63, no. 1, pp. 258–273, Jan. 2015.

[16] J. L. Williams and R. Lau, "Approximate evaluation of marginal association probabilities with belief propagation," *IEEE Trans. Aerosp. Electron. Syst.*, vol. 50, no. 4, pp. 2942–2959, Oct. 2014.

[17] P. Horridge and S. Maskell, "Using a probabilistic hypothesis density filter to confirm tracks in a multi-target environment," in *Proc. IEEE SDF-11*, Berlin, Germany, Oct. 2011.

[18] Y. Bar-Shalom and X.-R. Li, *Multitarget-Multisensor Tracking: Principles and Techniques*. Storrs, CT, USA: YBS Publishing, 1995.

[19] M. S. Arulampalam, S. Maskell, N. Gordon, and T. Clapp, "A tutorial on particle filters for online nonlinear/non-Gaussian Bayesian tracking," *IEEE Signal Process. Mag.*, vol. 50, no. 2, pp. 174–188, Feb. 2002.

[20] T. Li, M. Bolic, and P. M. Djuric, "Resampling methods for particle filtering: Classification, implementation, and strategies," *IEEE Signal Process. Mag.*, vol. 32, no. 3, pp. 70–86, May 2015.

[21] A. Smith, A. Doucet, N. de Freitas, and N. Gordon, *Sequential Monte Carlo Methods in Practice*. New York, NY, USA: Springer, 2013.

[22] Z. Botev, "Nonparametric density estimation via diffusion mixing," The University of Queensland, Tech. Rep., Nov. 2007. [Online]. Available: http://espace.library.uq.edu.au/view/UQ:120006

[23] J. H. Kotecha and P. M. Djuric, "Gaussian particle filtering," *IEEE Trans. Signal Process.*, vol. 51, no. 10, pp. 2592–2601, Oct. 2003.

[24] G. Gan, C. Ma, and J. Wu, *Data Clustering: Theory, Algorithms, and Applications*. Philadelphia, PA, USA: SIAM, 2007.

[25] D. Schuhmacher, B.-T. Vo, and B.-N. Vo, "A consistent metric for performance evaluation of multi-object filters," *IEEE Trans. Signal Process.*, vol. 56, no. 8, pp. 3447–3457, Aug. 2008.

[26] D. Musicki and R. Evans, "Joint integrated probabilistic data association: JIPDA," *IEEE Trans. Aerosp. Electron. Syst.*, vol. 40, no. 3, pp. 1093–1099, Jul. 2004.